



Synthesis and characterization of γ -Fe₂O₃/C nanocomposite as an efficient catalyst for the degradation of methylene blue

Gui-Yun Mao^a, Fan-Xing Bu^a, Wei Wang^a, Dong-Mei Jiang^a, Zhen-Jie Zhao^a,
Qing-Hong Zhang^b, Ji-Sen Jiang^{a,*}

^aDepartment of Physics, Center for Functional Nanomaterials and Devices, East China Normal University, Shanghai 200241, P.R. China, Tel. +86 21 54342931; emails: mg311@163.com (G.-Y. Mao), xueshuzhishang@163.com (F.-X. Bu), victorwang913@gmail.com (W. Wang), Tel. +86 21 54342940; email: dmjiang@phy.ecnu.edu.cn (D.-M. Jiang), Tel. +86 21 62233239; email: zjzhao@phy.ecnu.edu.cn (Z.-J. Zhao), Tel./Fax: +86 21 54342940; email: jsjiang@phy.ecnu.edu.cn (J.-S. Jiang)

^bEngineering Research Center of Advanced Glasses Manufacturing Technology, MOE, Donghua University, Shanghai 201620, P.R. China, Tel. +86 13916233742; email: zhangqh@dhu.edu.cn

Received 12 January 2014; Accepted 6 March 2015

ABSTRACT

Magnetic γ -Fe₂O₃/C nanocomposite was successfully synthesized by a facile approach in which Fe₃O₄/Starch was firstly obtained by one-pot precipitation method, and then starch was carbonized through calcination accompanied by the oxidation of Fe₃O₄ to γ -Fe₂O₃. The as-prepared γ -Fe₂O₃/C was introduced to the application of wastewater treatment, and methylene blue (MB) was used to simulate the oxidative degradation process of organic pollutants. Carbon coexisted in the γ -Fe₂O₃/C nanocomposite could well serve as a preconcentrator of MB dyes and consequently the catalytic performance was strongly enhanced. Moreover, the γ -Fe₂O₃/C catalyst could be easily recycled by magnetic separation for effective reuse. This work not only prepared γ -Fe₂O₃/C nanocomposite by a quite facile method, but also successfully employed it as a catalyst for degradation of organic pollutants under mild condition.

Keywords: γ -Fe₂O₃/C; Magnetic; Nanocomposite; Degradation; Wastewater treatment

1. Introduction

During past decades, industrial wastewater treatment has attracted widespread attention due to serious environmental issues. Various methods employing biological, physical, and chemical techniques, such as biotreatment, adsorption, and degradation, have been widely reported [1–9]. The degradation technique is more ideal for its convenient operational process, non-

secondary pollution, and preventing vast excess sludge [10–12]. The effective degradation of pollutants by oxidation processes is usually based on the generation of oxidizing reactive oxygen species such as hydroxyl radicals (\cdot OH), superoxide ions (\cdot O₂⁻), or singlet oxygen (¹O₂) [13–15]. \cdot OH radicals, generally produced from hydrogen peroxide (H₂O₂) in the presence of some catalysts, are especially highly active and nonselective in the oxidative degradation reaction with most of the organic pollutants. More importantly, the relevant procedures are totally eco-friendly; therefore,

*Corresponding author.

catalytic degradation reaction used for wastewater treatment has received intense research [16].

Nanoparticles of inorganic materials, such as metal oxides and semiconductors, have generated considerable attention due to their novel properties compared to their bulk materials. And several reports have shown that the material's photochemical and catalytic properties strongly depend on their particle size [17,18]. In recent years, Fe-based nanomaterials have been revealed to be outstanding candidates of heterogeneous catalysts owing to their large surface-to-volume area, high stability, and easy magnetic separation [10,19,20]. In order to further improve the catalytic capability, modifications have been made to embellish iron oxides materials for exceptional properties [5,10,11,20]. However, although high reaction rates are generally obtained with these catalytic systems, acidic environment, necessary activation process, and unknown recycle ability limit their use [21–25]. Therefore, it is attractive and desirable to exploit appropriate modification on Fe-based oxides to obtain some kind of materials that can overcome the above drawbacks.

In this work, we prepared $\gamma\text{-Fe}_2\text{O}_3/\text{C}$ nanocomposite with strong magnetic response by using one-pot starch-modifying method and subsequent heat treatment. Catalytic performances of the prepared $\gamma\text{-Fe}_2\text{O}_3/\text{C}$ nanocomposite in the oxidative degradation of methylene blue (MB) were studied. The influences of synthetic conditions and H_2O_2 content on the degradation efficiency of MB as well as recycle ability of the prepared samples were also investigated.

2. Experiment

2.1. Materials

Ferrous chloride ($\text{FeCl}_2 \cdot 4\text{H}_2\text{O}$), hydrogen peroxide (H_2O_2 30 wt%), dipropylamine ($\text{C}_6\text{H}_{15}\text{N}$), starch, and MB were purchased from Sinopharm Chemical Reagent Co., Ltd. All reagents and solvents were analytical grade and used as received without further purification unless otherwise indicated. Deionized water was used in the experiments throughout.

2.2. Preparation of $\text{Fe}_3\text{O}_4/\text{starch}$ nanoparticles

The $\text{Fe}_3\text{O}_4/\text{starch}$ nanoparticles were prepared by one-pot interface co-precipitation method, according to previous report with some modifications [26]. Firstly, 1.0 g starch was dissolved in 20 mL H_2O with vigorous mechanical stirring at 80°C in a water bath. Then, 0.8944 g $\text{FeCl}_2 \cdot 4\text{H}_2\text{O}$ was added in to get a light blue solution. Finally, 0.75 mL H_2O_2 (1 mol L^{-1}) was poured followed by 3 mL dipropyl amine and black

precipitate formed immediately. After constant stirring at 80°C for 2 h, the reaction was thoroughly finished. The precipitate was separated from the solution by an external magnet, and washed with ethanol and water till neutral. Then, the products were dried at 40°C in vacuum oven for 12 h.

2.3. Preparation of $\gamma\text{-Fe}_2\text{O}_3/\text{C}$ nanocomposite

The as-obtained $\text{Fe}_3\text{O}_4/\text{starch}$ nanoparticles were calcined at 250°C for 2 h at a heating rate of 2°C min^{-1} from room temperature (RT). In this process, the starch was carbonized to carbon; meanwhile, the Fe_3O_4 was oxidized to $\gamma\text{-Fe}_2\text{O}_3$. Thus, $\gamma\text{-Fe}_2\text{O}_3/\text{C}$ nanocomposite was obtained.

Pure $\gamma\text{-Fe}_2\text{O}_3$ was got by calcining Fe_3O_4 obtained at 80°C without addition of starch at 250°C for 2 h.

2.4. Characterization

The morphology of the products was investigated by a transmission electron microscope (TEM, JEM-2100) operated at 200 kV. X-ray diffraction (XRD) patterns were obtained with a Rigaku Ultima IV (D/tex) diffractometer using Cu $K\alpha$ radiation ($\lambda = 1.541 \text{ \AA}$). The transmission Mössbauer spectroscopy experiments were carried out in a constant acceleration with a 25 mCi⁵⁷Co (Pb) source at RT using 25 μm $\alpha\text{-Fe}$ foil as reference. The Mössbauer parameters were fitted by a standard least-squares fitting program. Fourier-transform infrared (FT-IR) spectra were measured in wavenumber ranging from 400 to $4,000 \text{ cm}^{-1}$ using a Nicolet Nexus 670 FT-IR spectrophotometer. The dried samples were grinded with KBr together, and then compressed into thin pellets for measurement. The Raman spectrum was taken on an inVia Reflex spectrometer (Renishaw) with an argon ion laser at an excitation wavelength of 514 nm. Mettler Toledo thermogravimetric and differential thermal combined analyzer (TGA/SDTA851e) was used to check out the thermal performance of the products with the temperature range from 25 to 700°C at a heating rate of $20^\circ\text{C min}^{-1}$ in air atmosphere. Nitrogen adsorption-desorption isotherms were examined using a Micromeritics ASAP 2010 M analyzer on the dried sample which had been degassed at 150°C under vacuum for 6 h. The Brunauer–Emmett–Teller (BET) specific surface area was calculated from the linear part of the BET plot. Pore size distribution was calculated using Barrett–Joyner–Halenda method. Magnetic hysteresis loops were obtained at RT using a Lakeshore 7400 model vibrating sample magnetometer under a magnetic field up to 12 kOe.

2.5. Catalysis test

Heterogeneous catalytic degradation reactions were carried out in an open batch reactor by shaking conical flasks at 20 °C and at the natural pH of the solution (pH 5.5). In a typical procedure, a certain amount of the product was homogeneously dispersed into MB solution and the solution was shaken for about 30 min to achieve adsorption equilibrium between the dye and the catalyst. Then, the degradation reaction was initiated by adding H₂O₂ into the solution. The final volume for all solutions was 30 mL (concentration of MB was 20 mg L⁻¹, and content of H₂O₂ was 29.1 mmol). At given intervals of degradation, an aliquot of MB solution was taken out and immediately separated with an external magnet. The absorbance intensity of the supernatant was measured at the maximum absorbance wavelength (665 nm) of the MB dye using a Unico UV-2802S ultraviolet and visible (UV-Vis) spectrophotometer. The concentration of MB was calculated by the standard curve in Fig. 1. The concentration of MB was calculated by this curve according to its absorbance value. And for solution of high concentration (abs > 1.0), dilution is needed to ensure the measurement accurate.

In order to validate the regenerative capacity and stability of γ -Fe₂O₃/C nanocomposite, the samples that collected from the reaction solution by a magnet were directly reused for the next cycle without any dispose, and the process was repeated for four times. The initial amount of γ -Fe₂O₃/C was 25 mg, and the reacting solution was 30 mL containing 20 mg L⁻¹ MB and 29.1 mmol H₂O₂, each cycle of reaction lasted 3 h.

The removal rate of MB for degradation ability judgment was calculated by C/C_0 [27].

The decomposition rate of H₂O₂ in the existence of catalyst was measured by titration with KMnO₄. In brief, an aliquot of H₂O₂ solution was taken out and

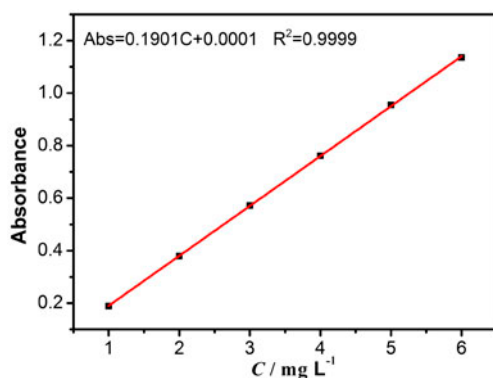


Fig. 1. The standard absorption curve of MB solution.

immediately separated with a magnet at given intervals. Supernatant of 0.5 mL was injured into 20 mL H₂O followed by adding 10 mL 3 M H₂SO₄ in a conical flask. Then, added KMnO₄ to the solution dropwise till the color turned to pink.

3. Results and discussion

3.1. Characterization of the samples

Fig. 2(a) shows a TEM image of the prepared γ -Fe₂O₃/C nanocomposite. In the image, the granular parts with dark color come from γ -Fe₂O₃ nanoparticles and the sheet-like parts with lighter contrast mean carbon. Thus, γ -Fe₂O₃ nanoparticles in the nanocomposite

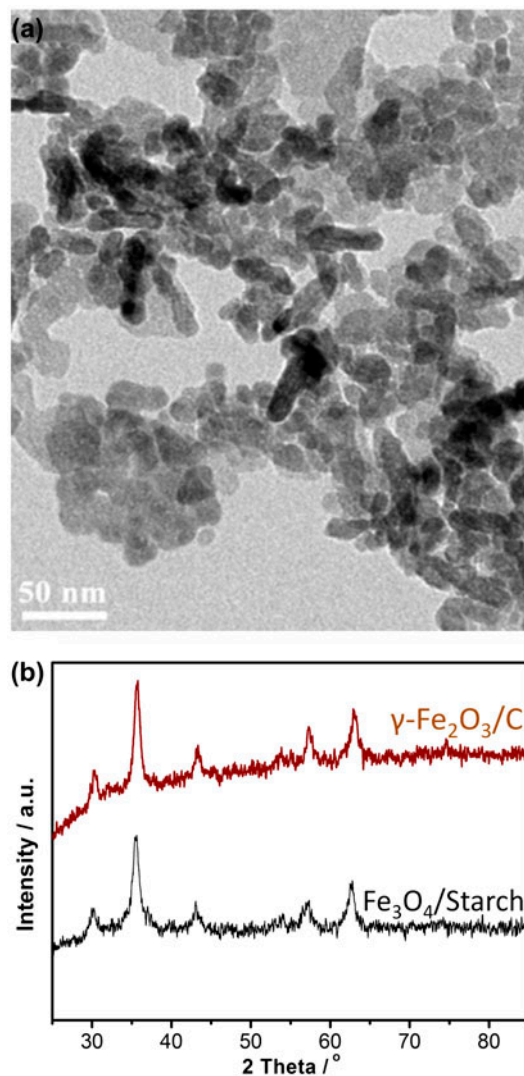


Fig. 2. (a) TEM micrograph of γ -Fe₂O₃/C; (b) XRD patterns of Fe₃O₄/starch and γ -Fe₂O₃/C.

are embedded in carbon. The size of $\gamma\text{-Fe}_2\text{O}_3$ particles was about 13 nm, and some particles aggregated might be due to their high surface activity under calcination process. Particle size of the obtained $\gamma\text{-Fe}_2\text{O}_3$ nanoparticles is about 12.4 nm according to Scherrer equation from XRD pattern in Fig. 2(b), which is consistent with the result of TEM. The XRD patterns in Fig. 2(b) match well with the inverse spinel structure of both $\gamma\text{-Fe}_2\text{O}_3$ (JCPDs:39-1346) [23,28] and Fe_3O_4 (JCPDs: 88-0315) [29]. No diffraction peaks due to carbon are observed in XRD pattern of $\gamma\text{-Fe}_2\text{O}_3/\text{C}$, indicating the amorphous nature and much lower content of carbon in the nanocomposite [30].

It is well known that it is difficult to identify $\gamma\text{-Fe}_2\text{O}_3$ and Fe_3O_4 by XRD spectra due to their similar structures, so we used Mössbauer spectroscopic analysis to determine the phase composition of the prepared samples. The Mössbauer spectra of the prepared samples at RT are given in Fig. 3, and the Mössbauer parameters of the samples are presented in Table 1. The spectrum for $\text{Fe}_3\text{O}_4/\text{Starch}$ clearly confirms the phase of Fe_3O_4 with isomer shift (I.S.) value of 0.40 mm s^{-1} for Fe^{3+} ions located in the tetrahedral sites (A-site) and 0.50 mm s^{-1} for $\text{Fe}^{2+}/\text{Fe}^{3+}$ ions located in the octahedral sites (B-site). The appearance

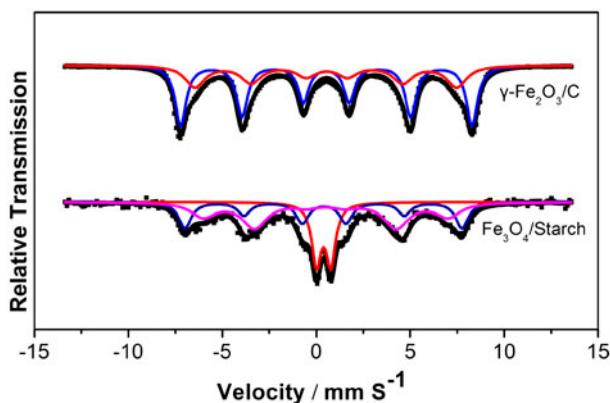


Fig. 3. RT Mössbauer spectra of $\text{Fe}_3\text{O}_4/\text{starch}$ and $\gamma\text{-Fe}_2\text{O}_3/\text{C}$.

of doublet reveals some particles in the $\text{Fe}_3\text{O}_4/\text{starch}$ composite are superparamagnetism [31]. Both hyperfine fields (456 kOe for iron ions in A-site and 403 kOe for iron ions in B-site) are lower than those of pure Fe_3O_4 , which may be caused by the fine particle size [32,33]. After the calcination of the $\text{Fe}_3\text{O}_4/\text{Starch}$ composite at 250°C , only I.S. values of 0.38 mm s^{-1} corresponding well with Fe^{3+} ions are observed in Mössbauer spectrum of the obtained sample. This indicates that all Fe^{2+} ions in Fe_3O_4 have been oxidized into Fe^{3+} ions to form $\gamma\text{-Fe}_2\text{O}_3$. The appearance of asymmetric broadening toward the central peak of Mössbauer spectrum for $\gamma\text{-Fe}_2\text{O}_3/\text{C}$ nanocomposite could be attributed to the surface effect [34,35] and the interaction between C and the surface of $\gamma\text{-Fe}_2\text{O}_3$. Doublet in Mössbauer spectrum of $\text{Fe}_3\text{O}_4/\text{starch}$ disappears after calcination at 250°C as shown in Mössbauer spectrum of sample $\gamma\text{-Fe}_2\text{O}_3/\text{C}$, indicating sample $\gamma\text{-Fe}_2\text{O}_3/\text{C}$ has no superparamagnetic behavior at RT. This may originate from the increased size of particles under calcination, which overpasses the smaller critical size 5 nm of $\gamma\text{-Fe}_2\text{O}_3$ [32].

The FT-IR spectra of the samples were measured to confirm the existence of carbon in the nanocomposite (Fig. 4(a)). The spectrum of $\text{Fe}_3\text{O}_4/\text{Starch}$ shows an absorption peak at 572 cm^{-1} , which corresponds to the symmetric vibration of Fe–O in Fe_3O_4 [35,36]. And $\gamma\text{-Fe}_2\text{O}_3/\text{C}$ shows strong peaks at 634 and 565 cm^{-1} , which are assigned to the vibration of the Fe–O functional group in $\gamma\text{-Fe}_2\text{O}_3$ [3,23,37]. This is well consistent with the Mössbauer spectra analysis. For $\text{Fe}_3\text{O}_4/\text{starch}$, the absorption at about $1,028 \text{ cm}^{-1}$ corresponds to asymmetric stretching vibration and flexural vibrations of C–O, while the peaks at about 3,413 and $1,401 \text{ cm}^{-1}$ can be attributed to O–H bending vibration and stretching vibration, implying the presence of starch in the sample [25,31]. In comparison with $\text{Fe}_3\text{O}_4/\text{starch}$, new peaks at 872 and $1,461 \text{ cm}^{-1}$ related to C=O [36,38] are formed in $\gamma\text{-Fe}_2\text{O}_3/\text{C}$ and peak at $2,925 \text{ cm}^{-1}$ belonged to C–H [37] becomes very weak, indicating the transformation from starch to carbon. Raman investigation of $\gamma\text{-Fe}_2\text{O}_3/\text{C}$ was used to further confirm the existence of carbon (Fig. 4(b)). The typical

Table 1
Mössbauer parameters of $\text{Fe}_3\text{O}_4/\text{starch}$ and $\gamma\text{-Fe}_2\text{O}_3/\text{C}$

Sample	Subspectra	Isomer shift (mm s^{-1})	Quadrupole splitting (mm s^{-1})	Hyperfine field (kOe)	Area rate
$\text{Fe}_3\text{O}_4/\text{starch}$	D	0.39 ± 0.01	0.77 ± 0.01	–	0.236 ± 0.011
	S1	0.40 ± 0.04	0.04 ± 0.03	456.55 ± 1.21	0.316 ± 0.024
	S2	0.50 ± 0.09	0.02 ± 0.05	403.71 ± 3.03	0.448 ± 0.026
$\gamma\text{-Fe}_2\text{O}_3/\text{C}$	S1	0.38 ± 0.02	0.00 ± 0.01	479.16 ± 0.55	0.708 ± 0.026
	S2	0.38 ± 0.08	0.06 ± 0.05	427.33 ± 3.02	0.292 ± 0.023

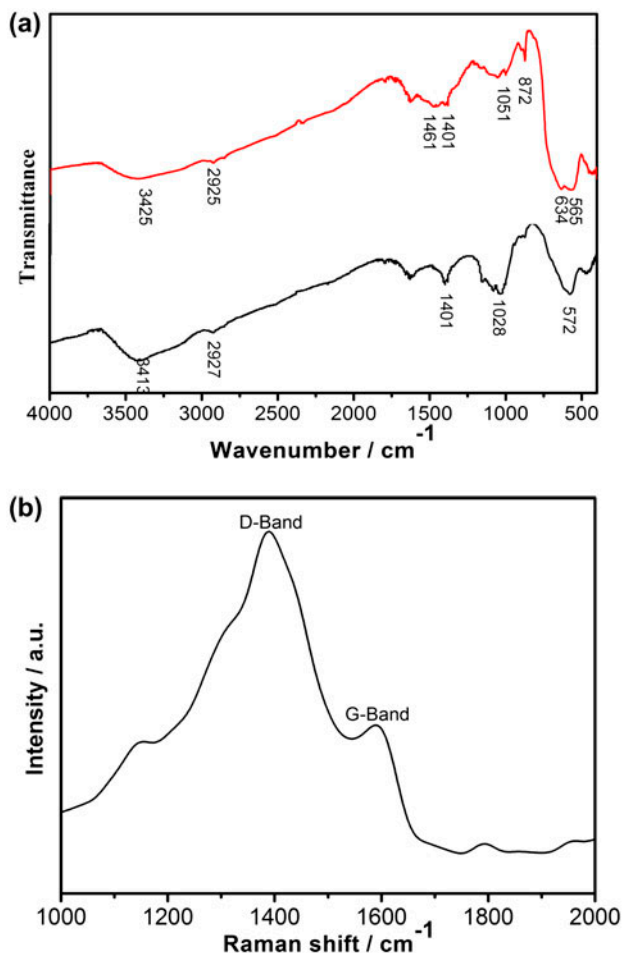


Fig. 4. (a) FT-IR spectra of $\text{Fe}_3\text{O}_4/\text{starch}$ and $\gamma\text{-Fe}_2\text{O}_3/\text{C}$; (b) Raman spectrum of $\gamma\text{-Fe}_2\text{O}_3/\text{C}$.

spectrum of $\gamma\text{-Fe}_2\text{O}_3/\text{C}$ exhibits two characteristic peaks centered at 1,390 and 1,589 cm^{-1} that are well in consistence with D-band and G-band of carbon. The intensity ratio of the two bands is $I_D/I_G = 2.13$, indicating the carbon is disordered [39,40]. All these results support the concept of carbonization of starch during heat treatment, and carbon is amorphous in the resulting nanocomposite.

TGA and SDTA carried out at a heating rate of $20^\circ\text{C min}^{-1}$ were used to further determine the chemical composition of the sample $\gamma\text{-Fe}_2\text{O}_3/\text{C}$ with $\gamma\text{-Fe}_2\text{O}_3$ as reference (Fig. 5). Nearly 0.9 and 3.0% weight loss was observed bellow 250°C for $\gamma\text{-Fe}_2\text{O}_3$ and $\gamma\text{-Fe}_2\text{O}_3/\text{C}$, respectively, due to evaporation of water that was physically adsorbed on the samples [41]. Weight loss of 3.0% means that $\gamma\text{-Fe}_2\text{O}_3/\text{C}$ contained more adsorbed water for its better adsorption ability. The weight loss of $\gamma\text{-Fe}_2\text{O}_3/\text{C}$ at $250\text{--}600^\circ\text{C}$ could be attributed mainly to the removal of C [30,38], thus the C

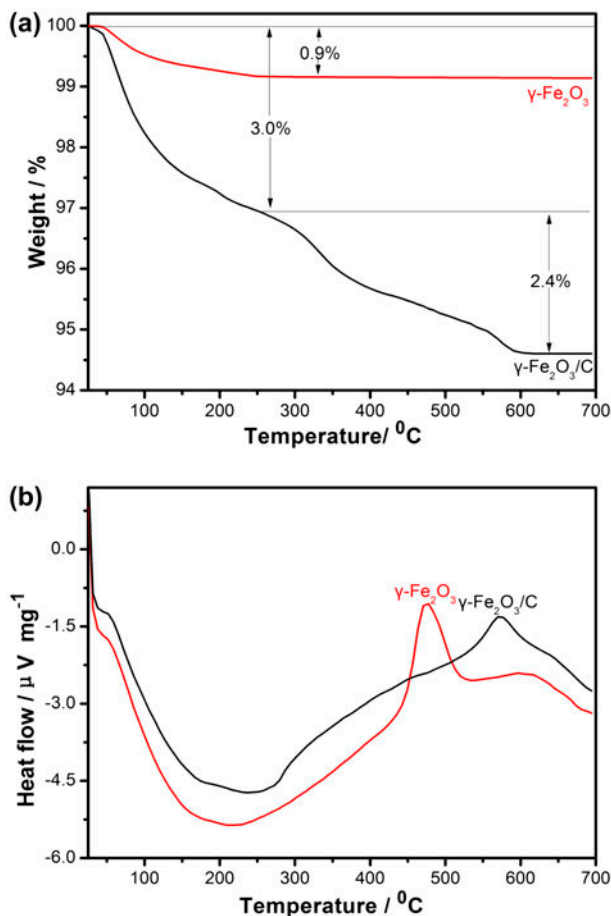


Fig. 5. TGA (a) and SDTA (b) curves of $\gamma\text{-Fe}_2\text{O}_3$ and $\gamma\text{-Fe}_2\text{O}_3/\text{C}$.

content of $\gamma\text{-Fe}_2\text{O}_3/\text{C}$ is determined to be about 2.4% by weight. SDTA was employed to further characterize the process of heat treatment (Fig. 5(b)). The SDTA curves of $\gamma\text{-Fe}_2\text{O}_3$ and $\gamma\text{-Fe}_2\text{O}_3/\text{C}$ show a wide endothermic peak at about 200°C , corresponding to the evaporation process of water. The exothermic peaks at 450 and 575°C that exhibit no counterparts on TGA reveals the phase transition from $\gamma\text{-Fe}_2\text{O}_3$ to $\alpha\text{-Fe}_2\text{O}_3$ [23,42] and the existence of C in $\gamma\text{-Fe}_2\text{O}_3/\text{C}$ increases the transition temperature.

Fig. 6 shows the N_2 adsorption–desorption isotherm and the pore size distribution curves of $\gamma\text{-Fe}_2\text{O}_3$ and $\gamma\text{-Fe}_2\text{O}_3/\text{C}$. The BET surface area of $\gamma\text{-Fe}_2\text{O}_3$ is $39.07\text{ m}^2\text{ g}^{-1}$ and the pore size distribution reveals a wide range centered at 22.3 nm. However, the $\gamma\text{-Fe}_2\text{O}_3/\text{C}$ has a much larger surface area of $116.54\text{ m}^2\text{ g}^{-1}$ and a relative narrow pore size distribution centered at 10.4 nm. A sharp inflection in the relative pressure (p/p_0) between 0.9 and 1.0 demonstrates the wide pore size distribution (see Fig. 6(a)) [43].

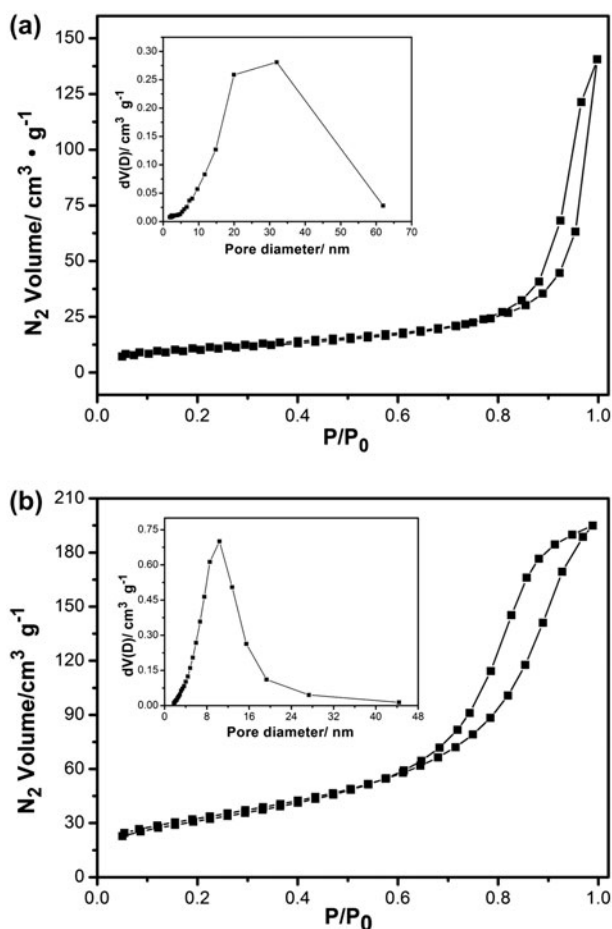


Fig. 6. N_2 adsorption–desorption isotherms and pore size distribution of (a) $\gamma\text{-Fe}_2\text{O}_3$ and (b) $\gamma\text{-Fe}_2\text{O}_3/\text{C}$.

However, for $\gamma\text{-Fe}_2\text{O}_3/\text{C}$, the position of adsorption–desorption curve is slightly shifted to lower values of p/p_0 , indicating decrease in the pore size (Fig. 6(b)) [18]. The N_2 adsorption results reveal that the modification of C resulted in an increase in the porosity of the sample compared with that of pure $\gamma\text{-Fe}_2\text{O}_3$. Without the protection of C, the $\gamma\text{-Fe}_2\text{O}_3$ particles would aggregate severely under thermal treatment, leading to a relative small surface area and wide size pore distribution. However, starch in $\text{Fe}_3\text{O}_4/\text{Starch}$ would be carbonated into porous carbon, which not only well protected particles from aggregation, but also had great contributions to the larger BET surface area of $\gamma\text{-Fe}_2\text{O}_3/\text{C}$.

The hysteresis loops of $\gamma\text{-Fe}_2\text{O}_3/\text{C}$ were measured in an applied magnetic field between -12 and 12 kOe at RT (Fig. 7). The saturated magnetization reaches 44.9 emu g^{-1} , implying a relative strong magnetic response to the external magnetic field [23]. Thus, the $\gamma\text{-Fe}_2\text{O}_3/\text{C}$ could be easily separated from the reaction

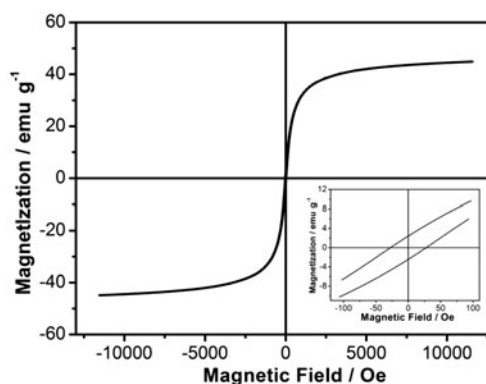


Fig. 7. Magnetic hysteresis loops of $\gamma\text{-Fe}_2\text{O}_3/\text{C}$ at RT.

system simply by magnetic separation after reaction. The inset of Fig. 7 shows that the coercivity force of $\gamma\text{-Fe}_2\text{O}_3/\text{C}$ is 27.4 Oe and the remanence is 2.3 emu g^{-1} , which indicates the nanocomposite is ferrimagnetic in consideration of Mössbauer spectra data. This result illustrates that the magnetic $\gamma\text{-Fe}_2\text{O}_3$ nanoparticles enwrapped by carbon keeps their intrinsic magnetic properties and crystal structure.

3.2. Catalytic degradation tests

The catalytic activity of $\gamma\text{-Fe}_2\text{O}_3/\text{C}$ nanocomposite was evaluated by the oxidation of MB with H_2O_2 in aqueous solution without pH adjustment. The MB dye was chosen for its high solubility, easy detection properties as well as having been widely studied as an important class of contaminant.

The absorption spectra curves of MB along with the reaction time of $\gamma\text{-Fe}_2\text{O}_3/\text{C}\&\text{H}_2\text{O}_2$ system are shown in Fig. 8(a). No new peaks are observed, which means a full oxidative decomposition of MB took place and no intermediates containing phenothiazine species were formed [44]. The inset of Fig. 8(a) shows excellent magnetic response of $\gamma\text{-Fe}_2\text{O}_3/\text{C}$ and the blue color almost disappeared after 180 min. Several contrast experiments were carried out for better understanding of the superior catalytic properties of the $\gamma\text{-Fe}_2\text{O}_3/\text{C}$ nanocomposite. The time profiles of MB decolorization under various reaction systems are displayed in Fig. 8(b) and the data were originated from the absorption at 665 nm. Neither as-prepared $\gamma\text{-Fe}_2\text{O}_3/\text{C}$ nor H_2O_2 alone showed apparent activity for MB degradation in 180 min. In contrast, remarkable MB decolorization occurred in $\gamma\text{-Fe}_2\text{O}_3\&\text{H}_2\text{O}_2$, $\text{Fe}_3\text{O}_4\&\text{H}_2\text{O}_2$, and $\gamma\text{-Fe}_2\text{O}_3/\text{C}\&\text{H}_2\text{O}_2$ suspension, and the $\gamma\text{-Fe}_2\text{O}_3/\text{C}$ even had better catalytic efficiency than the classic Fenton reagent Fe_3O_4 . The decomposition of H_2O_2 in this system and the influence of H_2O_2 content

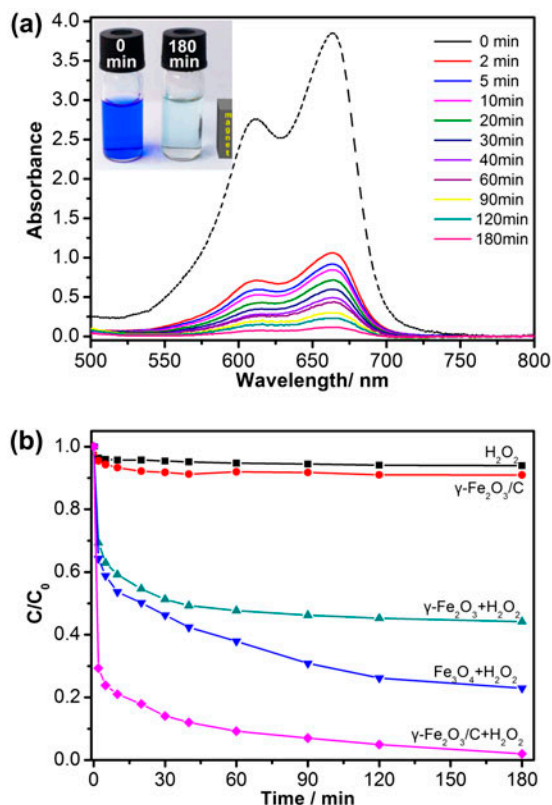


Fig. 8. (a) The change of MB absorption spectra for $\gamma\text{-Fe}_2\text{O}_3/\text{C}$ & H_2O_2 system and picture of MB solution before and after reaction (inset of a) (25 mg $\gamma\text{-Fe}_2\text{O}_3/\text{C}$, 29.1 mmol H_2O_2 , 20 mg L^{-1} MB); (b) Degradation of MB when using different catalysts (b: 25 mg solid material, 29.1 mmol H_2O_2 , 20 mg L^{-1} MB).

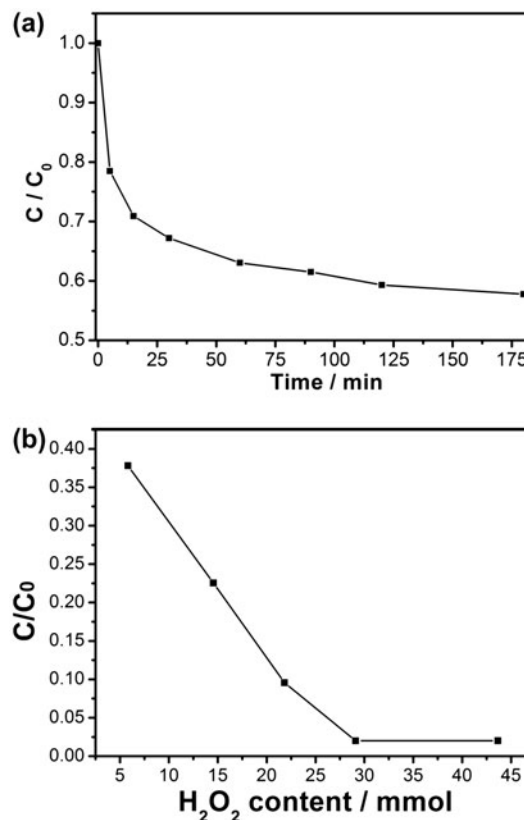


Fig. 9. (a) H_2O_2 decomposition in the existence of $\gamma\text{-Fe}_2\text{O}_3/\text{C}$ (25 mg $\gamma\text{-Fe}_2\text{O}_3/\text{C}$, 29.1 mmol H_2O_2); (b) effect of H_2O_2 content in the catalytic process on decolorization of MB (25 mg $\gamma\text{-Fe}_2\text{O}_3/\text{C}$, 20 mg L^{-1} MB, the reaction last 3 h).

in the catalytic process on the decolorization effect are shown in Fig. 9. The reaction rate of H_2O_2 decomposition in the $\gamma\text{-Fe}_2\text{O}_3/\text{C}$ & H_2O_2 system gradually became slower over time (Fig. 9(a)) and 29.1 mmol was revealed to be an appropriate H_2O_2 dosage, over which the degree of MB decolorization would not increase (Fig. 9(b)) due to the self-scavenging effect of H_2O_2 [18,19]. From Fig. 10, we can see that the higher is dosage of the $\gamma\text{-Fe}_2\text{O}_3/\text{C}$ nanocomposite, the better is the decolorization result, because more active sites are available at higher catalyst dosage. About 90% of MB was decolorized within 60 min when the content of $\gamma\text{-Fe}_2\text{O}_3/\text{C}$ reached 25 mg, indicating high decolorization activity of $\gamma\text{-Fe}_2\text{O}_3/\text{C}$ & H_2O_2 system.

Because calcination temperature and initial starch content influenced the composition and structure of the products in the thermal transformation process of solid phase, these two factors were optimized in this study. XRD patterns of samples obtained at different calcination temperatures and initial starch content are shown

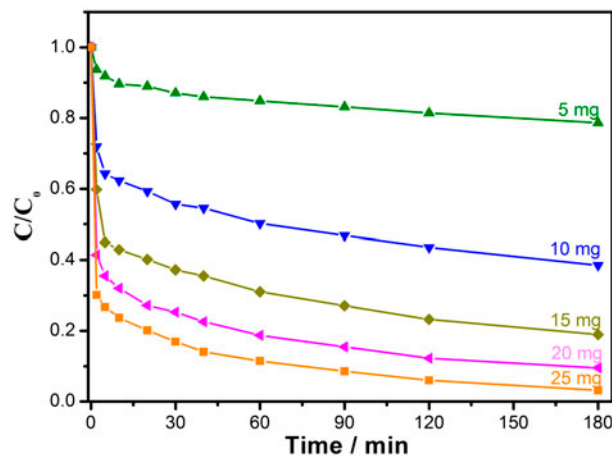


Fig. 10. Effect of $\gamma\text{-Fe}_2\text{O}_3/\text{C}$ content on decolorization of MB (29.1 mmol H_2O_2 , 20 mg L^{-1} MB).

in Fig. 11. It shows that all of them are inverse spinel structure. As clearly presented in Fig. 12(a), the sample obtained at 250°C has the best catalytic performance.

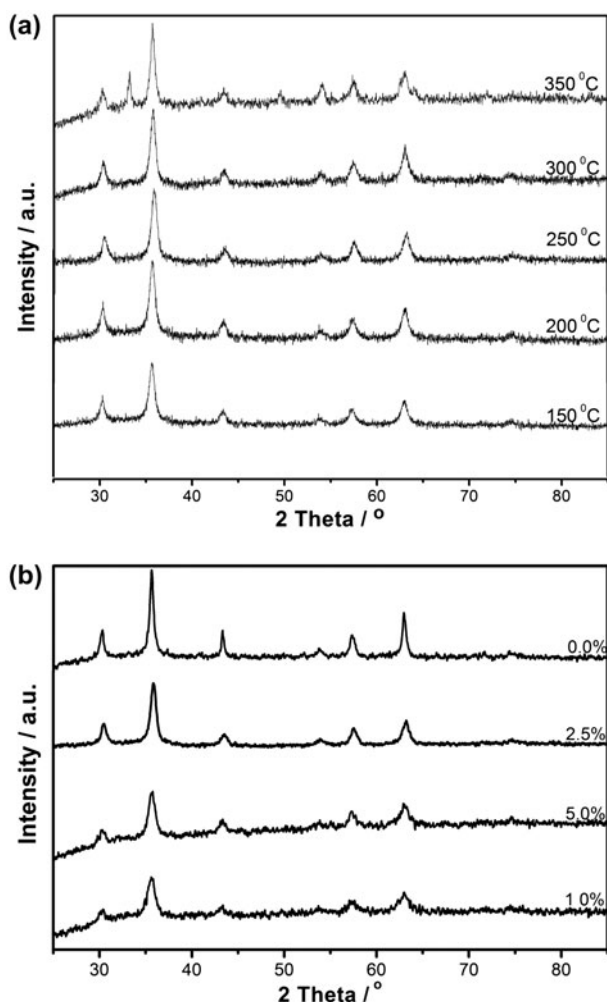


Fig. 11. XRD patterns of the samples calcinated at different temperatures (a) and the samples with different starch contents heated at 250 °C (b).

The reason for this result might be that Fe₃O₄/Starch was transformed into γ -Fe₂O₃/C successfully at this temperature as evidenced by Mössbauer spectra, FT-IR spectra, and Raman spectra data. And carbonization of starch as well as content of carbon was in good control [30]. With the increase in initial starch content, much more amorphous C was generated to improve the adsorption capacity of the nanocomposite and to increase the concentration of dyes near the surface of the catalyst for MB degradation [5,43], thus better catalytic performance was observed (Fig. 12(b)). However, when the starch content increased over 5 wt%, the catalytic active sites decreased because obtained C in the composite was too much and would cap the γ -Fe₂O₃ (C content > 2.4 wt%), resulting in the decrease of catalytic efficiency. This is a clear indication that the degradation process not only relates with the catalyst's surface area,

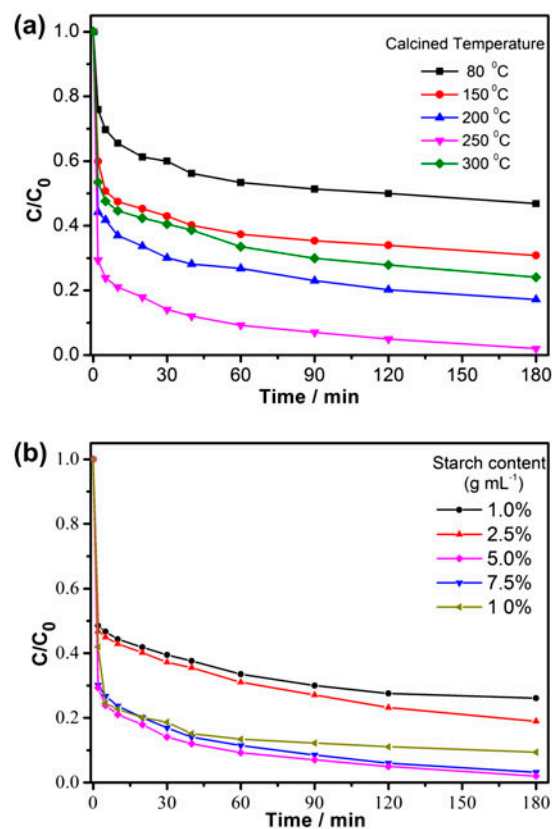
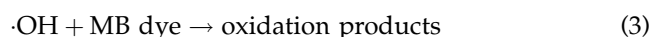
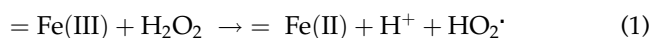


Fig. 12. Effects of synthetic conditions on degradation of MB (25 mg solid material, 29.1 mmol H₂O₂, 20 mg L⁻¹ MB) (a) calcined temperature and (b) initial starch content.

but also the content of γ -Fe₂O₃ active sites that is an important factor of catalytic degradation reaction [45].

Based on the results discussed above, we think the degradation of MB mainly contains two processes. Firstly, the MB molecules are adsorbed on the nanocomposite. And then the degradation reactions happen immediately to remove the MB after the injection of H₂O₂ into the system [43,46]. The reactions may proceed by Fenton-like process which is well known as production method of free hydroxyl radicals via the reaction of Fe together with H₂O₂, shown as the equations below (Eqs. (1) and (2)).



In all the above equations, = Fe(II) and = Fe(III) are iron species in the solid phase or at the solid-liquid interface. The produced free hydroxyl radicals (\cdot OH)

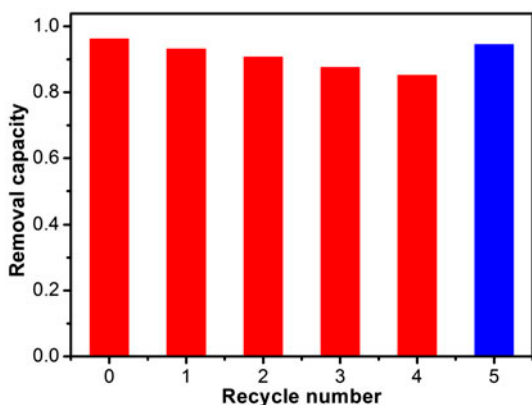


Fig. 13. Reuse ability of $\gamma\text{-Fe}_2\text{O}_3/\text{C}$ for degradation of MB (25 mg $\gamma\text{-Fe}_2\text{O}_3/\text{C}$, 29.1 mmol H_2O_2 , 20 mg L^{-1} MB, columns with red color mean the reaction last 3 h, while blue stands for 5 h).

degrade the organic pollutant MB dyes by breaking the benzene ring and relevant molecules in the structures to simple substances (Eq. (3)). That is how those MB molecules adsorbed on sorption sites are further degraded [43,47,48]. Several experiments revealed the MB discoloration reactions immediately stopped upon the removal of the catalyst from the medium by a simple magnetic separation. These results also clearly support a heterogeneous reaction initiated on the catalyst surface.

From the stand points of economic efficiency and environmental sustainability, it is essential to use renewable material to minimize the wastewater treatment cost. In view of this point, the regeneration and reusability of $\gamma\text{-Fe}_2\text{O}_3/\text{C}$ nanocomposite was tested to evaluate their application potential in the decontamination of MB-bearing wastewater. As shown in Fig. 13, it can be observed that in the first catalytic step, the removal rate of MB reached 97% in 3 h. With the increase in cycling times, the removal ability of MB decreased slightly, and can still reach 85% in 3 h at the fourth time. For comparison, we prolonged the reaction time of the last cycle to 5 h, and found the removal rate reached 95%, almost equal with the first time. The results clearly suggested good regeneration ability and sustainability of the $\gamma\text{-Fe}_2\text{O}_3/\text{C}$ nanocomposite.

4. Conclusions

By simply using one-pot starch-modifying synthesis and subsequent heat treatment method, we prepared $\gamma\text{-Fe}_2\text{O}_3/\text{C}$ nanocomposite. Serving as Fenton-like reagent, the $\gamma\text{-Fe}_2\text{O}_3/\text{C}$ was employed in the efficient and eco-friendly degradation of MB under mild condition. The tested MB solution (20 mg L^{-1}) was 90% decol-

orized in 60 min, and the degradation ratio reached 97% after 180 min. Moreover, the catalysts could be easily recycled by magnetic separation and reused without obvious activity decrease. Therefore, $\gamma\text{-Fe}_2\text{O}_3/\text{C}$ nanocomposite was obtained by a convenient method and was used as catalyst for decomposing H_2O_2 successfully. Moreover, C coexisted in the nanocomposite apparently enhanced the degradation performance of MB dyes. Consequently, $\gamma\text{-Fe}_2\text{O}_3/\text{C}$ nanocomposite showed good performance in the catalytic degradation of organic pollutants in wastewater treatment without tough conditions or secondary pollution.

Acknowledgments

This work was supported by the National Natural Science Foundation of China (Grant Nos. 21473059, 21173084) and Large Instruments Open Foundation of East China Normal University.

References

- [1] A. Demirbas, Heavy metal adsorption onto agro-based waste materials: A review, *J. Hazard. Mater.* 157 (2008) 220–229.
- [2] M.C. Pereira, F.S. Coelho, C.C. Nascentes, J.D. Fabris, M.H. Araújo, K. Sapag, L.C.A. Oliveira, R.M. Lago, Use of activated carbon as a reactive support to produce highly active-regenerable Fe-based reduction system for environmental remediation, *Chemosphere* 81 (2010) 7–12.
- [3] H. Zhu, R. Jiang, L. Xiao, W. Li, A novel magnetically separable $\gamma\text{-Fe}_2\text{O}_3/\text{crosslinked chitosan}$ adsorbent: Preparation, characterization and adsorption application for removal of hazardous azo dye, *J. Hazard. Mater.* 179 (2010) 251–257.
- [4] S. Yang, P. Zong, X. Ren, Q. Wang, X. Wang, Rapid and highly efficient preconcentration of Eu(III) by core-shell structured $\text{Fe}_3\text{O}_4/\text{humic acid}$ magnetic nanoparticles, *ACS Appl. Mater. Inter.* 4 (2012) 6891–6900.
- [5] C.C. Rezende, J.L. Neto, A.C. Silva, V.M. Lima, M.C. Pereira, L.C.A. Oliveira, Synthesis and characterization of iron/niobium composite: Catalyst for dye wastewater treatments, *Catal. Commun.* 26 (2012) 209–213.
- [6] C. Noubactep, Characterizing the discoloration of methylene blue in $\text{Fe}^0/\text{H}_2\text{O}$ systems, *J. Hazard. Mater.* 166 (2009) 79–87.
- [7] K. Miyajima, C. Noubactep, Impact of Fe^0 amendment on methylene blue discoloration by sand columns, *Chem. Eng. J.* 217 (2013) 310–319.
- [8] A.K. Hartash, C.P. Kaushik, Biodegradation aspects of polycyclic aromatic hydrocarbons (PAHs): A review, *J. Hazard. Mater.* 169 (2009) 1–15.
- [9] S. Jagadevan, N.J. Graham, I.P. Thompson, Treatment of waste metalworking fluid by a hybrid ozone-biological process, *J. Hazard. Mater.* 244–245 (2013) 394–402.
- [10] L. Kong, X. Gan, A.L. Ahmad, B.H. Hamed, E.R. Everts, B.S. Ooi, J. Lim, Design and synthesis of magnetic nanoparticles augmented microcapsule with

- catalytic and magnetic bifunctionalities for dye removal, *Chem. Eng. J.* 197 (2012) 350–358.
- [11] M.C. Pereira, L.C.A. Oliveira, E. Murad, Iron oxide catalysts: Fenton and Fenton-like reactions—A review, *Clay Miner.* 47 (2012) 285–302.
- [12] U.G. Akpan, B.H. Hameed, Parameters affecting the photocatalytic degradation of dyes using TiO₂-based photocatalysts: A review, *J. Hazard. Mater.* 170 (2009) 520–529.
- [13] Y.H. Ng, I.V. Lightcap, K. Goodwin, M. Matsumura, P.V. Kamat, To what extent do graphene scaffolds improve the photovoltaic and photocatalytic response of TiO₂ nanostructured films, *J. Phys. Chem. Lett.* 1 (2010) 2222–2227.
- [14] X. Shu, J. He, D. Chen, Visible-light-induced photocatalyst based on nickel titanate nanoparticles, *Ind. Eng. Chem. Res.* 47 (2008) 4750–4753.
- [15] T. Hirakawa, Y. Nosaka, Properties of O₂⁻ and OH⁻ formed in TiO₂ aqueous suspensions by photocatalytic reaction and the influence of H₂O₂ and some ions, *Langmuir* 18 (2002) 3247–3254.
- [16] L. Zhang, Y. Nie, C. Hu, X. Hu, Decolorization of methylene blue in layered manganese oxide suspension with H₂O₂, *J. Hazard. Mater.* 190 (2011) 780–785.
- [17] R.D. Stramel, Y.K. Thomas, Photochemistry of iron oxide colloids, *J. Colloid Interface Sci.* 110 (1986) 121–129.
- [18] A. Bach, G. Zelmanov, R. Semiat, Cold catalytic recovery of loaded activated carbon using iron oxide-based nanoparticles, *Water Res.* 42 (2008) 163–168.
- [19] K. Rusevova, F.D. Kopinke, A. Georgi, Nano-sized magnetic iron oxides as catalysts for heterogeneous Fenton-like reactions—Influence of Fe(II)/Fe(III) ratio on catalytic performance, *J. Hazard. Mater.* 241–242 (2012) 433–440.
- [20] R.C.C. Costa, F.C.C. Moura, J.D. Ardisson, J.D. Fabris, R.M. Lago, Highly active heterogeneous Fenton-like systems based on Fe⁰/Fe₃O₄ composite prepared by controlled reduction of iron oxides, *Appl. Catal., B* 83 (2008) 131–139.
- [21] H. Narayani, H. Arayapurath, S. Shukla, Using Fenton-reaction as a novel approach to enhance the photocatalytic activity of TiO₂-gamma-Fe₂O₃ magnetic photocatalyst undergoing photo-dissolution process without silica interlayer, *Catal. Lett.* 143 (2013) 807–816.
- [22] Z. Ai, Z. Gao, L. Zhang, W. He, J. Yin, Core-shell structure dependent reactivity of Fe@Fe₂O₃ nanowires on aerobic degradation of 4-chlorophenol, *Environ. Sci. Technol.* 47 (2013) 5344–5352.
- [23] L. Xu, J. Wang, Magnetic nanoscaled Fe₃O₄/CeO₂ composite as an efficient Fenton-like heterogeneous catalyst for degradation of 4-chlorophenol, *Environ. Sci. Technol.* 46 (2012) 10145–10153.
- [24] S. Xing, D. Zhao, W. Yang, Z. Ma, Y. Wu, Y. Gao, W. Chen, J. Han, Fabrication of magnetic core-shell nanocomposites with superior performance for water treatment, *J. Mater. Chem. A* 1 (2013) 1694–1700.
- [25] N. Ferroudj, J. Nzimoto, A. Davidson, D. Talbot, E. Briot, V. Dupuis, A. Bee, M.S. Medjram, S. Abramson, Maghemite nanoparticles and maghemite/silica nanocomposite microspheres as magnetic Fenton catalysts for the removal of water pollutants, *Appl. Catal., B* 136–137 (2013) 9–18.
- [26] B. Xu, H. Dou, K. Tao, K. Sun, J. Ding, W. Shi, X. Guo, J. Li, D. Zhang, K. Sun, “Two-in-One” fabrication of Fe₃O₄ /MePEG-PLA composite nanocapsules as a potential ultrasonic/MRI dual contrast agent, *Langmuir* 27 (2011) 12134–12142.
- [27] C. Jiang, Z. Gao, H. Qu, J. Li, X. Wang, P. Li, H. Liu, A new insight into Fenton and Fenton-like processes for water treatment: Part II. Influence of organic compounds on Fe(III)/Fe(II) interconversion and the course of reactions, *J. Hazard. Mater.* 250–251 (2013) 76–81.
- [28] S. Cao, Y. Zhu, Y. Zeng, Formation of γ -Fe₂O₃ hierarchical nanostructures at 500°C in a high magnetic field, *J. Magn. Magn. Mater.* 321 (2009) 3057–3060.
- [29] J. Xu, Y. Zhu, γ -Fe₂O₃ and Fe₃O₄ magnetically nanostructured hollow microspheres: Preparation, formation mechanism, magnetic property, and application in water treatment, *J. Colloid Interface Sci.* 385 (2012) 58–65.
- [30] T. Zhu, J. Chen, X. Lou, Glucose-assisted one-pot synthesis of FeOOH nanorods and their transformation to Fe₃O₄@carbon nanorods for application in lithium ion batteries, *J. Phys. Chem. C* 115 (2011) 9814–9820.
- [31] J.S. Jiang, Z.F. Gan, Y. Yang, B. Du, M. Qian, P. Zhang, A novel magnetic fluid based on starch-coated magnetite nanoparticles functionalized with homing peptide, *J. Nanopart. Res.* 11 (2009) 1321–1330.
- [32] R.É. Vandenberghe, E.D. Grave, C. Landuydt, Some aspects concerning the characterization of iron oxides and hydroxides in soils and clays, *Hyperfine Interact.* 53 (1990) 175–195.
- [33] N. Song, H. Yang, X. Ren, Z. Li, Y. Luo, J. Shen, W. Dai, X. Zhang, Z. Cheng, Non-monotonic size change of monodisperse Fe₃O₄ nanoparticles in the scale-up synthesis, *Nanoscale* 5 (2013) 2804–2810.
- [34] J.S. Jiang, X.L. Yang, L.W. Chen, N.F. Zhou, A Mossbauer study on the surface hyperfine field of uniform hematite particles, *Appl. Phys. A* 45 (1988) 245–247.
- [35] G.H. Jiang, J.S. Jiang, Preparation of γ -Fe₂O₃ nanoparticles by solid (wet)-phase grinding, *Chem. J. Chin. Univ.* 25 (2004) 405–408.
- [36] H. Liu, J. Zhuang, J. Yang, Preparation and application of core-shell Fe₃O₄/polythiophene nanoparticles, *J. Nanopart. Res.* 13 (2011) 6919–6930.
- [37] L. Xu, J. Dai, J. Pan, X. Li, P. Huo, Y. Yan, X. Zou, R. Zhang, Performance of rattle-type magnetic mesoporous silica spheres in the adsorption of single and binary antibiotics, *Chem. Eng. J.* 174 (2011) 221–230.
- [38] P. Wu, N. Du, H. Zhang, J. Yu, D. Yang, Carbon nanocapsules as nanoreactors for controllable synthesis of encapsulated iron and iron oxides: Magnetic properties and reversible lithium storage, *J. Phys. Chem. C* 115 (2011) 3612–3620.
- [39] Y. Zhang, M. Zhou, M. Fan, C. Huang, C. Chen, Y. Cao, H. Li, X. Liu, Improvement of the electrochemical properties of V₃O₇·H₂O nanobelts for Li battery application through synthesis of V₃O₇@C core-shell nanostructured composite, *Curr. Appl. Phys.* 11 (2011) 1159–1163.
- [40] X. Fan, G. Jiao, W. Zhao, P. Jin, X. Li, Magnetic Fe₃O₄-graphene composite as targeted drug nanocarriers for pH-activated release, *Nanoscale* 5 (2013) 1143–1152.
- [41] Z. Jing, Y. Wang, S. Wu, Preparation and gas sensing properties of pure and doped γ -Fe₂O₃ by an

- anhydrous solvent method, *Sens. Actuators B* 113 (2006) 177–181.
- [42] T. Zhang, H. Luo, H. Zeng, R. Zhang, Y. Shen, Synthesis and gas sensing characteristics of high thermostability γ -Fe₂O₃ powder, *Sens. Actuators B* 32 (1996) 181–184.
- [43] I.S.X. Pinto, P.H.V.V. Pacheco, J.V. Coelho, E. Lorencon, J.D. Ardisson, J.D. Fabris, P.P. de Souza, K.W.H. Krambrock, L.C.A. Oliveira, M.C. Pereira, Nanostructured δ -FeOOH: An efficient Fenton-like catalyst for the oxidation of organics in water, *Appl. Catal., B* 119–120 (2012) 175–182.
- [44] X. Liang, Y. Zhong, S. Zhu, L. Ma, P. Yuan, J. Zhu, H. He, Z. Jiang, The contribution of vanadium and titanium on improving methylene blue decolorization through heterogeneous UV-Fenton reaction catalyzed by their co-doped magnetite, *J. Hazard. Mater.* 199–200 (2012) 247–254.
- [45] X. Liang, Y. Zhong, H. He, P. Yuan, J. Zhu, S. Zhu, Z. Jiang, The application of chromium substituted magnetite as heterogeneous Fenton catalyst for the degradation of aqueous cationic and anionic dyes, *Chem. Eng. J.* 191 (2012) 177–184.
- [46] M.C. Pereira, L.C.D. Cavalcante, F. Magalhães, J.D. Fabris, J.W. Stucki, L.C.A. Oliveira, E. Murad, Composite prepared from natural iron oxides and sucrose: A highly reactive system for the oxidation of organic contaminants in water, *Chem. Eng. J.* 166 (2011) 962–969.
- [47] C. Wang, H. Liu, Z. Sun, Heterogeneous photo-Fenton reaction catalyzed by nanosized iron oxides for water treatment, *Int. J. Photoenergy* 2012 (2012) 1–10.
- [48] Y. Pang, A.Z. Abdullah, Effect of low Fe³⁺ doping on characteristics, sonocatalytic activity and reusability of TiO₂ nanotubes catalysts for removal of Rhodamine B from water, *J. Hazard. Mater.* 235–356 (2012) 326–335.